A new method for measuring deformation on volcanoes and other natural terrains using InSAR persistent scatterers

Andrew Hooper,[1] Howard Zebker,[1] Paul Segall,[1] and Bert Kampes[2]

[1] We present here a new InSAR persistent scatterer (PS) method for analyzing episodic crustal deformation in non-urban environments, with application to volcanic settings. Our method for identifying PS pixels in a series of interferograms is based primarily on phase characteristics and finds low-amplitude pixels with phase stability that are not identified by the existing amplitude-based algorithm. Our method also uses the spatial correlation of the phases rather than a well-defined phase history so that we can observe temporally-variable processes, e.g., volcanic deformation. The algorithm involves removing the residual topographic component of flattened interferogram phase for each PS, then unwrapping the PS phases both spatially and temporally. Our method finds scatterers with stable phase characteristics independent of amplitudes associated with man-made objects, and is applicable to areas where conventional InSAR fails due to complete decorrelation of the majority of scatterers, yet a few stable scatterers are present. *INDEX TERMS:* 1243 Geodesy and Gravity: Space geodetic surveys; 1294 Geodesy and Gravity: Instruments and techniques; 6924 Radio Science: Interferometry; 8494 Volcanology: Instruments and techniques. **Citation:** Hooper, A., H. Zebker, P. Segall, and B. Kampes (2004), A new method for measuring deformation on volcanoes and other natural terrains using InSAR persistent scatterers, *Geophys. Res. Lett.*, *31*, L23611, doi:10.1029/2004GL021737.

1. Introduction

[2] A major limitation in our ability to model volcanic processes is the lack of deformation data for most active volcanoes. While conventional InSAR has proven very effective in measuring deformation in regions of good coherence [e.g., *Massonnet et al.*, 1995; *Amelung et al.*, 2000], it is clear from almost any volcano interferogram that there are large areas on most volcanoes where signals decorrelate and no measurement is possible. If the surface is vegetated, weathers appreciably or is prone to snow coverage, the scattering properties change with time and result in temporal decorrelation, i.e., the loss of interferogram coherence with time [*Zebker and Villasenor*, 1992]. Another limitation of existing InSAR methods is the lack of temporal resolution in the data. While to a large extent this limitation is a function of how often SAR data are acquired, there are two other aspects of conventional InSAR that limit

the number of scenes from which interferograms can be produced. The first is the distance between the spacecraft tracks at the two times scenes are acquired, known as the perpendicular baseline. A non-zero baseline leads to a difference in incidence angle which alters the scattering phases, a phenomenon referred to as spatial decorrelation [*Zebker and Villasenor*, 1992]. As the baseline increases, spatial decorrelation also increases. A second limitation results from the changes in squint angle, the angle with which the spacecraft is looking forward or backward. A change in squint angle alters the SAR Doppler frequency and leads to additional decorrelation. Although these non-temporal causes of decorrelation can be reduced somewhat by filtering, there are critical values of baseline and squint angle difference beyond which there is complete loss of interferogram coherence [*Zebker and Villasenor*, 1992].

[3] The degree of decorrelation of radar signals depends on the distribution of scattering centers within a pixel. If the phase of a pixel were determined by just one stable point scatterer, the decorrelation would be reduced to zero. Although this is never the case for real surfaces, there are pixels which behave somewhat like point scatterers, and for which decorrelation is greatly reduced. Hence, in an interferogram some pixels will exhibit less decorrelation than others. It is possible to avoid many limitations of conventional InSAR by analyzing only pixels which retain some degree of correlation, which we define as persistent scatterers.

[4] A different approach to processing is required to identify and isolate these pixels. This approach was first realized for InSAR applications by *Ferretti et al.* [2000, 2001], with further enhancements by *Colesanti et al.* [2003], and is referred to as the Permanent Scatterers Technique™ in their patented procedure. Other persistent scatterer processing systems have since been developed [e.g., *Adam et al.*, 2003; *Crosetto et al.*, 2003; *Lyons and Sandwell*, 2003; *Werner et al.*, 2003]. In these algorithms, an initial set of PS pixels are identified by analysis of their amplitude scintillations in a series of interferograms. This method works best in urban areas where man-made structures increase the likelihood of finding a non-fluctuating scatterer in any given pixel. The density of PS pixels identified by this technique in natural terrains, however, is generally too low to obtain any reliable results. Our new method uses phase analysis for identification of PS pixels and is successfully applied to a volcanic area where, using the *Ferretti et al.* [2001] algorithm, we failed to find an initial set of PS pixels with sufficient density to be reliable.

[5] In order to estimate and remove nuisance terms, PS processing systems to date must simultaneously estimate the deformation for each PS, which requires a first-order model for the temporal deformation. Once the nuisance terms have

---

[1]Department of Geophysics, Stanford University, Stanford, California, USA.

[2]Remote Sensing Technology Institute, German Aerospace Center (DLR), Oberpfaffenhofen, Wessling, Germany.

been removed, higher-order deviations from the model may be estimated [*Ferretti et al.*, 2000; *Colesanti et al.*, 2003]. However, in the case of volcanoes, deformation tends to be episodic and not readily parameterized. In contrast, our method produces a time series of deformation, with no prior assumptions about its temporal nature. This is achieved by using the spatially correlated nature of the deformation rather than requiring a known temporal dependence.

2. Method

2.1. Persistent Scatterer Selection

[6] Because PS are defined by phase stability, we select PS candidates on the basis of their phase characteristics. Existing methods for selecting PS candidates rely on thresholding pixel amplitude dispersion with time, defined as the ratio of the standard deviation of the amplitude over its mean [*Ferretti et al.*, 2001]. For high (>10) signal to noise ratio (SNR), amplitude dispersion is an accurate proxy for phase standard deviation and thus the method has a high success rate at picking bright PS, e.g., certain man-made structures. However, for low SNR scatterers, the simple relationship between amplitude dispersion and phase stability breaks down and the method is no longer effective.

[7] Our approach is to form interferograms and remove most of the topographic phase signature using a digital elevation model (DEM). The residual phase, ϕ, of the xth pixel in the ith topographically corrected interferogram can be written as the sum of 5 terms,

$$\phi_{x,i} = \phi_{def,x,i} + \phi_{\alpha,x,i} + \phi_{orb,x,i} + \phi_{\varepsilon,x,i} + n_{x,i} \qquad (1)$$

where ϕ_{def} is the phase change due to movement of the pixel in the satellite line-of-sight (LOS) direction, ϕ_α is the phase equivalent of the difference in atmospheric retardation between passes, ϕ_{orb} is the phase due to orbit inaccuracies, ϕ_ε is the residual topographic phase due to error in the DEM and n is the noise term due to variability in scattering from the pixel, thermal noise and coregistration errors. We define PS as pixels where n is small enough that it does not completely obscure the signal.

[8] Variation in the first four terms of equation (1) can dominate the noise term making it difficult to identify which scatterers are persistent. We assume that ϕ_{def}, ϕ_α and ϕ_{orb} are spatially correlated over distances of a specified length scale, L, and that ϕ_ε and n are uncorrelated over the same distance, with a mean of zero. If the positions of other PS are already known, averaging the phase of all those within a circular patch centered on pixel x with radius L implies

$$\bar{\phi}_{x,i} = \bar{\phi}_{def,x,i} + \bar{\phi}_{\alpha,x,i} + \bar{\phi}_{orb,x,i} + \bar{n}_{x,i} \qquad (2)$$

where the bar denotes the sample mean of the patch and $\bar{n}$ is the sum of the sample means of n and ϕ_ε and is assumed small. Subtracting equation (2) from equation (1) leaves

$$\phi_{x,i} - \bar{\phi}_{x,i} = \phi_{\varepsilon,x,i} + n_{x,i} - \bar{n}'_{x,i} \qquad (3)$$

where $\bar{n}' = \bar{n} + (\bar{\phi}_{def} - \phi_{def}) + (\bar{\phi}_\alpha - \phi_\alpha) + (\bar{\phi}_{orb} - \phi_{orb})$.

[9] The phase error from uncertainty in the DEM is proportional to the perpendicular component of the baseline, $B_\perp$, so $\phi_{\varepsilon,x,i} = B_{\perp,x,i}K_{\varepsilon,x}$ where K_ε is a proportionality

constant. Substituting this expression into equation (3) we are able to estimate K_ε for pixel x in a least square sense, as this is the only term that would correlate with baseline. We define a measure based on the temporal coherence of pixel x as $\gamma_x = (1/N)|\sum_{i=1}^{N} \exp\{j(\phi_{x,i} - \bar{\phi}_{x,i} - \hat{\phi}_{\varepsilon,x,i})\}|$ where N is the number of available interferograms and $\hat{\phi}_{\varepsilon,x,i}$ is our estimate of $\phi_{\varepsilon,x,i}$. Assuming $\bar{n}'_{x,i}$ values are small, γ_x is a measure of the phase stability of the pixel and hence an indicator of whether the pixel is a PS.

[10] Because the algorithm requires PS phases to calculate the patch mean, it can identify PS given that the locations of other PS are already known. As we start with no knowledge of the location of any PS, we use an iterative algorithm to identify PS in all locations simultaneously. For computational reasons, we make an initial selection of PS candidates based on amplitude dispersion with a high threshold value (0.4). Unlike the initial selection in the *Ferretti et al.* [2001] algorithm, the vast majority of those selected are not actually PS. For each PS candidate, we subtract the mean of the other local candidates as in equation (3), estimate $K_{\varepsilon,x}$ and calculate γ_x. Generally, $\bar{n}'_{x,i}$ will not be negligible as the signal of the majority of the PS candidates included in the mean phase will be dominated by noise. Statistically, however, pixels with higher γ_x are more likely to be PS. Hence we temporarily reject candidates with low γ_x and recalculate the patch means using only the remaining candidates. We then recalculate γ_x for every candidate. Generally the values of $\bar{n}'_{x,i}$ will be smaller than before and by iterating a number of times the contribution of $\bar{n}'_{x,i}$ is gradually reduced so that γ_x becomes dominated by $n_{x,i}$.

[11] The final step is to select PS based on the calculated values of γ_x. Any pixel with random phase has a finite chance of having high γ_x and therefore we can only select in a probabilistic fashion. We therefore find a threshold value γ^* that maximizes the number of real PS selected while keeping the fraction of random phase pixels selected (false positives) below a specified value, q. The probability density function (PDF) of γ_x for the data, $p(\gamma_x)$, is a weighted sum of the PDF for the random phase pixels, $p_r(\gamma_x)$, and the PDF for the non-random phase (PS) pixels, $p_{ps}(\gamma_x)$ i.e., $p(\gamma_x) = (1 - \alpha)p_r(\gamma_x) + \alpha p_{ps}(\gamma_x)$. We want to find γ^* such that $(1 - \alpha)\int_{\gamma^*}^{1}p_r(\gamma_x)d\gamma_x/\int_{\gamma^*}^{1}p(\gamma_x)d\gamma_x = q$, where $p_r(\gamma_x)$, and α are unknown. $p_r(\gamma_x)$ is simulated by generating pseudo-PS candidates with random phase, estimating $K_{\varepsilon,x}$ for each and calculating γ_x. For low γ_x values (<0.3), $p_{ps}(\gamma_x) \approx 0$. Assuming then that $\int_{0}^{0.3}p(\gamma_x)d\gamma_x = (1 - \alpha)\int_{0}^{0.3}p_r(\gamma_x)d\gamma_x$ allows a conservative value of α to be estimated and hence we can calculate γ^*.

[12] Since the risk of false positives increases with increasing amplitude dispersion, we refine the number of PS selected further by calculating γ^* as a function of amplitude dispersion. For each PS candidate we then use the value of γ^* which corresponds to the amplitude dispersion of the candidate as the threshold value.

[13] In order to exclude sidelobes we assume that adjacent selected pixels are dominated by the same scatterer, and discard all but the pixel with the highest γ_x value.

2.2. DEM Error Correction

[14] Once the PS have been selected, their phase is corrected for DEM error by subtracting the estimated values of $\phi_{\varepsilon,x,i}$,
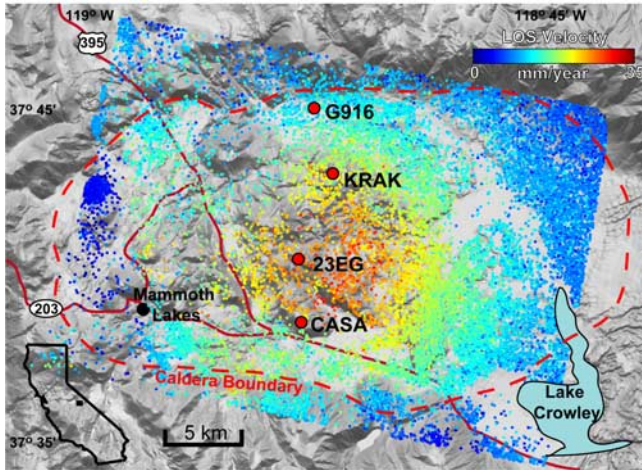
Figure 1. Location of Long Valley Caldera in California and the PS identified within the study area superimposed on a shaded relief map. The color of each PS represents the mean velocity in LOS.

$$\phi_{x,i} - \hat{\phi}_{\varepsilon,x,i} = \phi_{def,x,i} + \phi_{\alpha,x,i} + \phi_{orb,x,i} + \phi'_{\varepsilon,x,i} + n_{x,i} \qquad (4)$$

where $\phi'_{\varepsilon,x,i}$ is the residual DEM error term due to uncertainty in our estimate of $K_{\varepsilon,x}$, including any spatially correlated DEM error. Because the differential error between neighboring PS introduced by this spatially correlated error is small, the effect on unwrapping (see below) is negligible. However, the cumulative effect over larger areas could be significant so this spatially correlated part is estimated and removed as described in Section 2.4.

2.3. Unwrapping

[15] As long as the density of PS is such that the absolute phase difference between neighboring PS, after correction for estimated DEM error, is generally less than π, the corrected phase values can now be unwrapped. In this analysis the unwrapping problem is in three dimensions (two spatial, as with conventional InSAR, and one temporal), for which no efficient algorithms have yet been developed. Therefore we approach the unwrapping as a series of 2D problems. First, we calculate the temporal
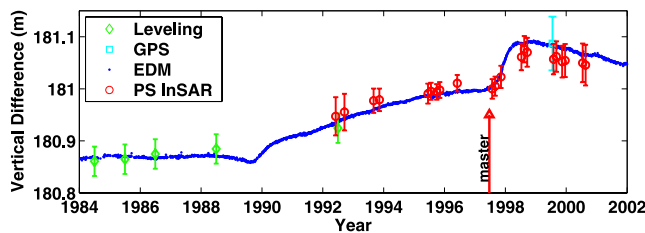
Figure 2. Comparison of vertical motion between benchmarks 23EG and G916 (see Figure 1) from leveling and GPS to PS (calculated from the mean phase of all PS within 500 m of the benchmarks). The error bars represent 68% confidence bounds. Also shown is the scaled line length change between CASA and KRAK as measured by EDM, which is a proxy for vertical motion.

phase differences for each PS, and then for each time step we unwrap spatially from a reference PS using an iterative least square method. Integrating in time then gives us an unwrapped phase time series for each PS, with respect to the reference PS. This method is sufficient to map slow deformation over time and a full 3D solution will likely be required if large displacements occur.

### 2.4. Spatially Correlated Terms

[16] After unwrapping, four error terms remain in equation (4) which mask ϕ_{def}. Unlike ϕ_{def}, the spatially correlated portion of these terms is assumed to be uncorrelated temporally. Thus, by high-pass filtering the unwrapped data in time then low-pass filtering in space we are able to estimate the spatially correlated error (similar to *Ferretti et al.* [2001]). Subtracting this signal from equation (4) leaves just ϕ_{def} and spatially uncorrelated error terms that can be modeled as noise.

3. Application

[17] We applied our method to data acquired over Long Valley Volcanic Caldera in eastern California (see Figure 1). This is an area largely devoid of man-made objects and has deformed at an irregular rate since ERS data was first acquired there in 1992 (see Figure 2). For short temporal and perpendicular baselines, conventional interferometry works well within the caldera [*Fialko et al.*, 2001], providing a comparison for our new method (see Figure 3). The deformation of the caldera is also extensively monitored by other means allowing us to validate the technique. We processed 22 descending scenes acquired by ERS1 and ERS2 between 1992 and 2000, and oversampled by a factor of two in range and azimuth to avoid aliasing in an amplitude based registration algorithm. We then selected one scene as the "master" (based primarily on minimization of perpendicular baseline and secondarily on minimization
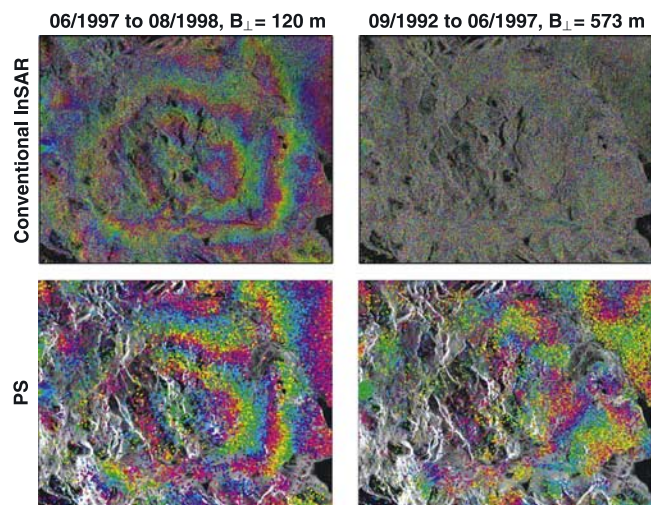
Figure 3. Comparison of wrapped multilooked interferograms from (top) conventional InSAR and (bottom) the wrapped phase of individual PS, corrected for DEM error. For the conventional interferograms 4 looks were taken in range and 20 in azimuth.
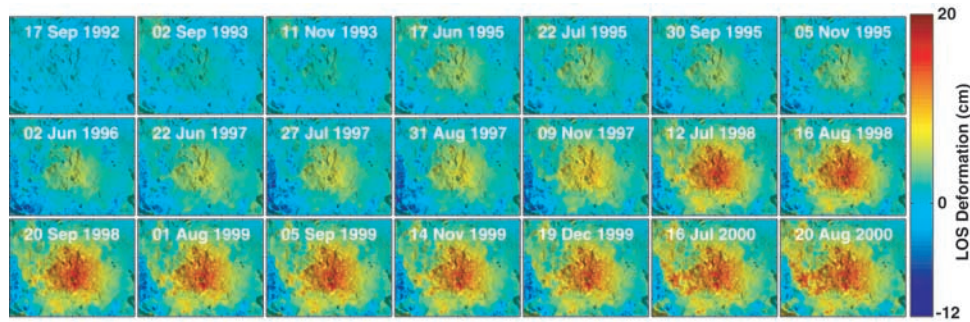
Figure 4. Time series of deformation interpolated spatially from the processed PS, referenced temporally to the earliest scene (04-Jun-1992), referenced spatially to the northeast corner and superimposed on the mean amplitude image.

of temporal baseline) and created 21 interferograms from each of the others.

[18] Using amplitude dispersion thresholding [*Ferretti et al.*, 2001] the density of PS identified over most of our region of interest was <0.1 km^{-2}, which is too low to provide reliable results. However, with our new algorithm we identified an average 44 km^{-2} with 95% confidence (see Figure 1). Figure 3 shows a sample comparison of the wrapped phase from conventional interferometry to the corrected phase of only the selected PS. In the shorter baseline (both perpendicular and temporal) case the results are comparable while in the longer baseline case there is considerably more spatial coherence using the new method.

[19] From the PS phases we calculated a time series of deformation between benchmarks 23EG and G916, assuming that all the detected relative motion was vertical, and compared it to that measured by leveling and GPS, and inferred from electronic distance meter (EDM) measurements (see Figure 2). Motion measured by the EDM line between CASA and KRAK is almost parallel to the satellite track and hence not present in our interferograms. However, this horizontal motion across the resurgent dome is almost proportional to the vertical motion of the resurgent dome [*Battaglia et al.*, 2003] and, once scaled using less frequent leveling and GPS readings, is therefore a proxy for vertical deformation. PS measurements are indistinguishable from ground truth at 68% confidence. If we relax our unrealistic assumption that all the relative motion is vertical and estimate east-west motion that is proportional to the vertical motion, the fit becomes even better. The time series of deformation for the whole processed region is shown in Figure 4.

[20] It is important to understand that except for true point scatterers, being a PS is not a physical characteristic of a pixel, but rather a function of the pixel and the dataset. As true point scatterers are rare even in urban areas, PS picked by any method are only point-like in their observed scattering characteristics. As the longest perpendicular baseline in the Long Valley data is 573 m, it is possible that some of the selected PS are less point-like in their scattering characteristics than would be conventionally termed PS. However, we can state that for at least 95% of the selected pixels, the signal is statistically distinguishable from the noise (our definition of a PS). If we used interferograms with longer baselines, this may no longer be true for the least point-like of the currently selected PS and

they would no longer be selected as PS. In other words our method will pick the largest possible set of PS from any given dataset.

4. Conclusions

[21] We have developed a method for identifying and processing PS that i) is applicable to low-amplitude natural targets and ii) requires no prior model of deformation. Using this method, we identified 44 PS km^{-2} in a non-urban volcanic area, for which we failed to get any reliable results using the method of *Ferretti et al.* [2001]. From these PS we were able to extract the temporal and spatial pattern of deformation even where conventional interferograms showed almost complete decorrelation. Although the pattern of temporal deformation is irregular, our method was able to extract it without any prior assumptions about its nature.

[22] While we have demonstrated the effectiveness of this method for the study of volcanic deformation, it is equally applicable to other deformation regimes such as fault slip, landslides and subsidence.

References

Adam, N., B. Kampes, M. Eineder, J. Worawattanamateekul, and M. Kircher (2003), The development of a scientific permanent scatterer system, paper presented at ISPRS Hannover Workshop, Inst. for Photogramm. and Geoinf., Hannover, Germany.

Amelung, F., S. Jonsson, H. Zebker, and P. Segall (2000), Widespread uplift and ''trapdoor'' faulting on Galapagos volcanoes observed with radar interferometry, *Nature*, 407, 993–996.

Battaglia, M., P. Segall, J. Murray, P. Cervell, and J. Langbein (2003), The mechanics of unrest at Long Valley caldera, California: 1. Modeling the geometry of the source using GPS, leveling and two-color EDM data, *J. Volcanol. Geotherm. Res.*, 127(3–4), 195–217.

Colesanti, C., A. Ferretti, F. Novali, C. Prati, and F. Rocca (2003), SAR monitoring of progressive and seasonal ground deformation using the permanent scatterers technique, *IEEE Trans. Geosci. Remote Sens.*, 41, 1685–1701.

Crosetto, M., A. Arnaud, J. Duro, E. Biescas, and M. Agudo (2003), Deformation monitoring using remotely sensed radar interferometric data, paper presented at 11th FIG Symposium on Deformation Measurements, Patras Univ., Santorini, Greece.

Ferretti, A., C. Prati, and F. Rocca (2000), Nonlinear subsidence rate estimation using permanent scatterers in differential SAR interferometry, *IEEE Trans. Geosci. Remote Sens.*, 38, 2202–2212.

Ferretti, A., C. Prati, and F. Rocca (2001), Permanent scatterers in SAR interferometry, *IEEE Trans. Geosci. Remote Sens.*, *39*, 8–20.

Fialko, Y., M. Simons, and Y. Khazan (2001), Finite source modelling of magmatic unrest in Socorro, New Mexico, and Long Valley, California, *Geophys. J. Int.*, *146*(1), 191–200.

Lyons, S., and D. Sandwell (2003), Fault creep along the southern San Andreas from interferometric synthetic aperture radar, permanent scatterers, and stacking, *J. Geophys. Res.*, *108*(B1), 2047, doi:10.1029/2002JB001831.

Massonnet, D., P. Briole, and A. Arnaud (1995), Etna monitored by space-borne radar interferometry, *Nature*, *375*, 567–570.

Werner, C., U. Wegmüller, T. Strozzi, and A. Wiesmann (2003), Interferometric point target analysis for deformation mapping, paper presented at International Geoscience and Remote Sensing Symposium, Toulouse, France.

Zebker, H. A., and J. Villasenor (1992), Decorrelation in interferometric radar echoes, *IEEE Trans. Geosci. Remote Sens.*, *30*, 950–959.

———————————

A. Hooper, P. Segall, and H. Zebker, Department of Geophysics, Mitchell Building, Stanford University, Stanford, CA 94305, USA. (ahooper@stanford.edu)

B. Kampes, Remote Sensing Technology Institute, German Aerospace Center (DLR), Muenchner Strasse 20, Oberpfaffenhofen, Wessling D-82234, Germany.